Defective UiO-66(Zr) as an efficient catalyst for the synthesis of bio jet-fuel precursors via aldol condensation of furfural and MIBK

Daniel de la Flor,[a] Clara López-Aguado,[a] Marta Paniagua,[a] Gabriel Morales,[a] Rafael Mariscal,[b] Juan A. Melero[a]*

[a] Chemical and Environmental Engineering Group. Universidad Rey Juan Carlos, C/Tulipán s/n. Móstoles. 28933 Madrid, Spain

[b] Energy and Sustainable Chemistry (EQS) Group. Institute of Catalysis and Petrochemistry, CSIC, Marie Curie 2, Campus de Cantoblanco. 28049 Madrid, Spain

KEYWORDS: Bio-jet fuel; Lignocellulose; Furfural; Aldol condensation; UiO-66; Zirconium; MOF

* Corresponding author:

E-mail: juan.melero@urjc.es

Phone-number: +34-91 488 73 99

Abstract

The production of jet-fuel precursors from furfural (FUR) via aldol-condensation with methyl-isobutyl ketone (MIBK) over a defective UiO-66(Zr) catalyst is presented. The resultant C11 adduct (FuMe) would allow the selective production of branched alkanes in the range of jet fuel via a subsequent hydrogenation/hydrodeoxygenation process. The catalyst is prepared using formic acid as modulator, leading to the incorporation of defects on the microcrystalline structure of the metalorganic framework (MOF) material, which dramatically boosts the catalytic performance in this transformation. Thus, the benchmarking with different commercial solid acid catalysts and Zr-based heterogeneous catalysts has identified the defective MOF, UiO-66(Zr)-FA, as clearly superior. An extensive characterization of the modified catalyst by means of X-ray diffraction (XRD), argon adsorption isotherm, thermogravimetry (TGA), acid titration, X-ray photoelectron spectroscopy (XPS), and diffuse reflectance infrared Fourier transform (DRIFT) of adsorbed deuterated acetonitrile, has confirmed the incorporation of missing-linker and missing-node defects within the structure, enabling to explain the enhancement in the catalytic process. The analysis of the reaction kinetics, together with the optimization of the reaction conditions by means of a response surface methodology (allowing predicting the behaviour of the catalytic system under very different conditions) have identified the temperature as the most relevant parameter affecting the selectivity to FuMe. Thus, under the optimized reaction conditions (130 °C; 4 h; FUR/Cat = 2; MIBK/FUR = 4), outstanding total FUR conversion and FuMe selectivity (~100%) can be achieved. However, the catalyst gets progressively deactivated in successive catalytic runs under the studied reaction conditions, which is attributed to the formation of organic deposits coming from furfural side reactions.

1. Introduction

Decarbonizing the energy system is critical to reach the ambitious global climate objectives. Among the different sectors, transport accounts for a significant portion of the greenhouse gas (GHG) emissions, ca. 25% (Data & Statistics, IEA). To achieve climate neutrality, the most favourable scenarios foresee the necessity of about 90% reduction in transport GHG emissions by 2050. However, far from decreasing in the last few years, emissions from transport keep increasing with respect to the 1990 baseline. This is especially true for the aviation sector, the one with the fastest growth. In this context, the European Union has recently released "The European Green Deal",[1] presenting a preliminary roadmap of key policies and measures needed to transform the EU economy, aiming at a sustainable future. In this strategy, the ramping-up of the production and deployment of sustainable alternative fuels, in particular for long-distance transport sectors such as aviation, marine, rail, and long-distance trucking -that are yet hard to electrify- appears as one of the priorities. Particularly, advanced biofuels are among the alternatives for introducing sustainable and renewable energy for transport. This category represents biofuels produced from non-food related and sustainable feedstock, such as energy crops, algae, and biomass wastes, as well as agricultural and forestry residues.

Lignocellulosic materials constitute the most abundant source of renewable biomass, being fully available from low-cost agriculture and forestry residues. The use of non-edible lignocellulosic biomass is thus a highly appealing alternative for the production of advanced biofuels with reduced, or even neutral, environmental impact. However, lignocellulose conversion into advanced biofuels is not a trivial task because of its chemical and structural variety and complexity, elevated stability, and high oxygen content. One of the main challenges is to transform this complex raw feedstock into synthetic fuels with a carbon length matching that of gasoline (C_5-C_{13}), diesel (C_{10}-C_{25}), and jet-fuel (C_{10}-C_{16}), so-called drop-in biofuels. Advantageously, such biofuels are functionally equivalent to petroleum fuels and hence fully compatible with existing infrastructure. Different approaches have been described in the literature to transform lignocellulose main components (cellulose, hemicellulose, and lignin) into synthetic fuels. Conventional gasification followed by a Fischer-Trop (FT) catalytic process is one of the most studied alternatives. However, FT still has several challenges to solve, such as syngas clean up, catalyst contamination, and economy of scale. Other well-documented alternative is the pyrolysis of lignocellulosic biomass to yield bio-oil and its subsequent catalytic hydrodeoxygenation (HDO), process requiring an intensive use of hydrogen and harsh reaction conditions. Indeed, pyrolysis route is not yet applied at large-scale due to numerous limitations, including the low yields of the final upgraded bio-oils and the fast deactivation of the catalysts. In this context, catalytic upgrading of sugars coming from the hydrolysis of cellulose and hemicellulose carbohydrates towards the production of synthetic fuels has received great attention in the last years [2–4].

Cellulose and hemicellulose carbohydrates can be depolymerized to the corresponding C5 and C6 sugars, but such compounds need to be further processed to increase the carbon-chain length up to the range of conventional fuels, as well as to reduce the oxygen content [5]. Thus, it is necessary to first obtain the so-called "platform molecules" -such as 5-hydroxymethylfurfural (5-HMF), furfural, and levulinic acid, among others- and then promote C-C bonding reactions (e.g., aldol condensation, hydroalkylation, ketonization, oligomerization, etc.). Then, the removal of oxygen through catalytic HDO reactions would finally yield the desired drop-in biofuels. The mild reaction conditions of this route in comparison with the thermocatalytic processes (gasification and pyrolysis) a priori ensure a higher product selectivity with lower energy consumption. Although the conversion of carbohydrates to furfural and levulinic acid has been well described in the literature, and even some commercial routes have been developed,[6] the subsequent production of transport fuel-range hydrocarbons through C-C coupling reactions remains poorly addressed.[2–5]

Furfural, which is already commercialized from the dehydration of xylose-rich materials, has a global market volume of 652 500 tons per year, with an average price of 1250-2100 $ per ton.[6] Aldol-condensation is a widely used method to build C-C bonds between two carbonyl-containing compounds with a reactive α-H atom on at least one of them, as in the case of furfural. Several works dealing with the catalytic conversion of furfural to fuel precursors via aldol-condensation have been published.[7,8,17–19,9–16] Most of them focus on the use of the simplest ketone, the acetone,[7,8,10–14] but its fossil origin (as by-product of the cumene process), as well as its small size (C2), limit the applicability thereof for the production of sustainable transportation fuel components. Therefore, the most recent studies tend to use larger and branched ketones such as cyclopentanone[15–18] and methyl isobutyl ketone (MIBK).[9,19]

In aldol condensation reactions, base catalysts are typically used, being the homogeneous bases -such as NaOH and KOH- among the most utilized. However, these catalysts can hardly be recycled and lead to corrosion and environmental concerns.[12–14,16,17] In order to minimize such drawbacks, solid base catalysts such as Mg-Al and Mg-Zr mixed oxides, La & Zn-based catalysts, and CaO have also been tested.[7–9,19,20] An additional attempt in the same line has been the preparation of carbon hybrid basic metal oxides with graphene-oxide hybrid zirconium MOFs as precursors, applied to the aldol condensation of furfural and MIBK. However, due to the low activity of α-H atom of MIBK, this reaction can only be catalyzed by strong solid bases, being difficult to design and synthesize hybrid solid bases to afford above requirement.[21] Additionally, poor stability under reaction conditions has been reported for all the mentioned base materials, leading to a significant leaching of active species. On the other hand, it is known that aldol condensation can proceed via acid catalysis too. The use of Brønsted acid catalysts (e.g., Nafion, Amberlyst-15, Amberlyst-36, H-USY, ZSM-5, H-Beta) has shown low selectivity towards the desired condensation adducts due to the formation of humins.[18] Lewis acid catalysts such as Hf-, Sn-, and Zr-loaded Beta zeolites and Sn-MFI have also been explored in the aldol

condensation of furfural with acetone.[10,11] Unlike Brønsted acid sites, weaker Lewis acid sites seem to catalyse selectively aldol condensation reactions avoiding the formation of undesired polymeric compounds.

Metal-organic frameworks (MOFs) are three-dimensional reticular structures, highly porous and crystalline, consisting of organic bridging ligands covalently bonded in coordination to metal ions or metal ion clusters.[22,23] They combine high metal concentrations with high porosity and surface areas, within well-defined and uniform structures, allowing the presence of multiple and periodic active sites. Therefore, they have emerged as an interesting alternative to conventional heterogeneous catalysts,[24,25] particularly in the promotion of biomass transformations, with superior catalytic performances.[26,27] Typical concerns in the catalytic application of MOFs include their somehow limited thermal, chemical and/or mechanical stabilities in the relatively harsh reaction conditions needed in many real applications. Therefore, current research is focused on MOF materials displaying enhanced resistance properties. In this regard, zirconium-based MOFs feature exceptional thermal, chemical, and mechanical stabilities.[28,29] Among them, UiO-66(Zr) has received considerable attention in the last decade due to an easy lab-scale synthesis as well as high stability.[30] Likewise, the structural properties of UiO-66(Zr) can be tailored through defect engineering, bringing beneficial changes to the catalytic activity. The incorporation of modulators during the synthesis to compete with the linkers binding the Zr_6 clusters has been broadly explored to generate defects in the framework.[31] Thus, defects introduced in UiO-66(Zr) material have been proposed to increase the accessibility and activity of the Zr clusters as moderate Lewis acid sites in some catalytic reactions.[24,32] Such an enhanced catalytic behaviour might also be considered for the efficient aldol condensation of furfural with ketones. Therefore, within this manuscript we present for the first time the preparation of biofuel precursors via the aldol condensation of biomass-derived furfural and MIBK over a defective Zr-based UiO-66 MOF. The catalytic performance of this material is benchmarked with other solid catalysts, either base or acid, especially considering Zr-based materials (Zr-SBA-15; ZrO_2-SBA-15; Zr-Beta and Zr-USY) displaying Lewis acidity. The effect of various reaction parameters (reaction temperature, catalyst loading, and MIBK to furfural molar ratio) both in the furfural conversion and the selectivity towards the oxygenated adduct are thoroughly analysed. Moreover, the kinetics of the aldol condensation reaction over the modified UiO-66(Zr) catalyst, as well as stability and reusability thereof, are explored.

2. Experimental

2.1 Catalysts preparation

The synthesis of the standard UiO-66(Zr), displaying few defects, was performed as first described by Cavka et al via solvothermal synthesis using zirconium chloride and terephthalic acid in dimethyl formamide (DMF).[28] Typically, $ZrCl_4$ (1.92 g, Merck, 98%) and DMF (100 mL, Quimipur, 99.8%), were stirred to get a homogeneous

solution. Terephthalic acid (1 g, Merck, 98%), was then added to the solution and stirring was continued for 90 min. The resultant mixture was introduced in a Teflon-lined stainless-steel autoclave to be hydrothermally aged at 120 °C for 48 h. The precipitated solid was recovered by centrifugation in acetone (5x) and then dried at 110 °C overnight. A modified version of this MOF was prepared employing formic acid (FA, Merck, 96%) as a modulator to generate defects in the framework during the construction of the crystalline solid. The synthesis of the FA-modulated UiO-66(Zr) material -herein denoted as UiO-66(Zr)-FA- was accomplished following the procedure described by Cliffe et al[33] adapted to Zr instead of Hf: $ZrCl_4$ (1.92 g, Merck, 98%) was added to a DMF:FA (80:20 vol.%) mixture and stirred until total dissolution. From here, the procedure is as above indicated for the UiO-66(Zr) sample.

ZrO_2-grafted mesostructured SBA-15 silica (ZrO_2-SBA-15) was prepared according to the method described by Osatiashtiani et al[34]: purely siliceous SBA-15 (10 g, prepared as in the original procedure of Zhao et al[35]) was pre-dried at 300 °C for 4 h before refluxing with zirconium propoxide (58.5 g, 70 wt.% in isopropanol, Merck) overnight in anhydrous hexane (300 mL, 95%, Merck). The amount of zirconium precursor was estimated from the concentration of hydroxyl groups on the SBA-15 silica surface determined from thermo-gravimetric analysis, in order to achieve a conformal monolayer of zirconia. The resultant solid was filtered and washed three times with hexane to remove any unreacted species, and rehydrated in deionised water (300 mL) under stirring for 4 h to fully hydrolyse the residual propoxide moieties. The material was filtered and dried at 80 °C overnight, and finally calcined for activation at 550 °C in static air for 3 h.

Zr-SBA-15 catalyst was synthesised following the procedure optimized by Melero et al[36]. Zirconocene dichloride, Cp_2ZrCl_2 (99%, ABCR), was used as metal precursor to incorporate isolated Zr species within the silica mesostructure during the synthesis. The template surfactant Pluronic 123 (4 g, Aldrich) was dissolved in 0.63 N HCl aq. solution (125 mL) at r.t., and thereafter zirconocene dichloride was added (Si/Zr ratio = 10) and stirred at 40 °C for 3h. Tetraethylorthosilicate (TEOS, 98%, Merck) was then added and stirred for 20 h at 40 °C. The resultant white suspension was transferred to an autoclave and hydrothermally aged at 130 °C for 24 h. Afterwards, the solid obtained by filtration was dried overnight and finally calcined (450 °C, 5 h) in order to remove the surfactant from the porous structure.

Zr-modified Beta zeolites were synthesized following a two-step procedure previously optimized by our group[37], dealuminating a commercial Beta zeolite (Zeolyst, Si/Al 19) and afterwards grafting Zr species into the generated tetrahedral vacancies, using zirconium nitrate (Chemical Point) as metal precursor. Three different dealumination grades were achieved by attacking the zeolite with HNO_3 in order to extract aluminum from the zeolite (0.1-10M, r.t. and 100 °C, 1-20 h, 20 mL g^{-1}). After filtration and washing with deionized water, the resulting materials were oven-dried overnight. Subsequently, the dealuminated Beta zeolites were suspended in deionized water (10 mL g^{-1}) followed by the addition of the appropriate amount of $Zr(NO_3)_4$. Water was removed from the resultant slurry under vacuum, and the remaining solid was dried overnight and

calcined in air (200 °C, 6 h, and then 550 °C, 6 h). Three Zr-modified Beta zeolites were synthesized and named Zr-Beta(X), X denoting the Al/Zr molar ratio. Likewise, Zr-modified USY zeolite (Zr-USY) was synthesized using an equivalent procedure to that of zeolite Beta but starting from a commercial H-USY zeolite (Zeolyst, Si/Al 8.4), as previously reported.[38]

Furthermore, as reference catalysts, commercial solid catalysts were also evaluated in this work. These included the acidic macroporous resin, Amberlyst-15 (Sigma-Aldrich); commercial acid zeolites (H-USY, Si/Al 8.4; H-Beta, Si/Al 19) provided by Zeolyst; and calcium oxide (CaO, Merk) and zirconium oxide (ZrO_2, Merck) used as solid base and Zr-based references, respectively, for the synthesized catalysts.

2.2 Catalyst characterization

Textural properties of the synthesized materials have been determined from nitrogen adsorption-desorption isotherms, recorded at 77 K using a Micromeritics TRISTAR 3000 system. Surface area values were calculated from isotherm data using the BET method and total pore volume was taken at P/P_o=0.975 single point. In the case of microporous materials (zeolites and MOFs), a Quantachrome AutoSorb 1 MP instrument was employed to record the argon adsorption-desorption isotherms at 87 K. Pore size distributions were calculated from the adsorption branch of the argon isotherms by applying the Non Local Density Functional Theory (NLDFT) model, assuming argon adsorption in cylindrical pores. Structural characterization was completed by X-ray powder diffraction (XRD) patterns, which were acquired on a Philips X-pert diffractometer using the Cu Kα radiation (λ = 1.5418 Å), and recording data at different 2θ angles depending on the sample, at low angle to determine mesoscopic ordering in the SBA-15 materials and at high angle for crystalline materials (zeolites and MOFs). Zr and Al contents were determined by means of Inductively-Coupled Plasma-Optical Emission Spectroscopy (ICP-OES) on a Varian Vista AX apparatus. Thermogravimetric analyses (TGA) were accomplished in an SDT 2960 Simultaneous DSC-TGA, from TA Instruments with 100 mL/min air flow rate and 5 °C/min heating ramp. X-ray Photoelectron Spectroscopy (XPS) measurements were obtained using a XPS Physical Electronics PHI 5700 photoelectron spectrometer using non-monochromatic Al-Kα radiation (300 W, 15 kV and 1486.6 eV). Binding energy values were referenced to carbon C1s peak (284.8 eV). Diffuse reflectance infrared Fourier transform (DRIFT) spectra were collected with a Nicolet 5700 spectrometer equipped with an Hg-Cd-Te cryodetector, working in the spectral range of 4000-650 cm^{-1}. A Praying Mantis (Harrick Co) as a mirror optical accessory was fitted. Deuterated acetonitrile (CD_3CN) was used as molecular probe to evaluate surface acidity. Samples were placed in a high temperature catalytic reaction chamber (Harrick Scientific Products, NY) that allows treatment in situ at high temperature. MOF materials were previously treated at 120 °C for 1 h under an argon flow (50 mL min^{-1}) to clean the surface. Thereafter, an argon flow carrying CD3CN was passed through the sample until saturation. Removal of physisorbed molecular probe was performed by heating under Ar flow. All spectra were recorded with 128 scans accumulation and a resolution of 4 cm^{-1}.Potentiometric titration experiments were performed on UiO-66(Zr) samples. In a typical procedure, 50 mg of sample was added to 60

mL of 0.01M $NaNO_3$ solution and stirred for 18 h to promote cationic exchange. Then, pH value was adjusted to 3.0 by adding 0.1M aq. HCl, and the titration was carried out by dropwise addition of 0.1 M aq. NaOH until pH 11.

2.3 Catalytic tests

Catalytic tests of aldol condensation of furfural (FUR, Merck, 99%) and methyl isobutyl ketone (MIBK, Merck, 99.5%) were performed in liquid phase in a stainless-steel stirred autoclave (30 mL) fitted with temperature control and a pressure gauge. MIBK and FUR were mixed in different molar ratios, using the ketone in excess (from 1:1 to 6:1, respectively). Sulfolane (Merck, 99%) was used as internal standard in a sulfolane:FUR molar ratio of 1:10. Catalysts were added to the solution in a FUR:Cat mass ratio ranging from 2:1 to 10:1. Once the reaction mixture was brought to the selected temperature (in the range 110-170 °C), stirring was initiated and set at 1000 rpm in order to avoid mass transfer limitations. Reusability experiments were performed recovering the spent catalyst by filtration and applying a mild washing procedure with acetone at room temperature to remove remaining organic species from the catalyst pores. The resultant powder was then dried overnight at 110 °C before being reused in a new reaction cycle.

2.4 Products analysis

Reaction samples were analysed by means of GC in an Agilent 7820A Gas Chromatograph, using a CP-WAX 52 CB column (30 m, 0.25 mm, 0.25 μm) and a FID detector. Chemical compounds detected by GC included unreacted species of FUR and MIBK, the standard sulfolane, and the condensation products, mainly that coming from the reaction of 1 molecule of furfural with 1 molecule of MIBK, herein denoted as FuMe. In certain reactions, the further condensation product of FuMe with another molecule of MIBK, denoted as $Fu(Me)_2$, was also identified (Scheme 1). Likewise, depending on the catalyst and reaction conditions applied, some other minor unidentified compounds were observed in the chromatograms, which have been attributed to the formation of soluble humins.

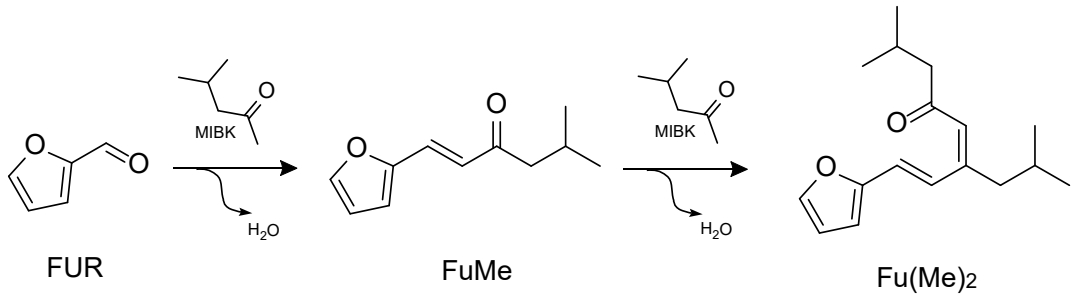

Scheme 1. Aldol condensation of furfural (FUR) with methyl isobutyl ketone (MIBK), to give the respective adducts, FuMe and $Fu(Me)_2$.

Furfural quantification was based on a calibration of the GC analysis unit with standard stock solution of the pure commercially available chemical. For the calibration of FuMe, non-commercially available, its chemical synthesis and purification was performed according to the process described by Pholjaroen et al [9] using CaO as catalyst to achieve total conversion of FUR, followed by evaporation under vacuum of the remaining MIBK. FuMe structure was confirmed using ^{1}H NMR and ^{13}C NMR analysis (Bruker Avance III/500 spectrometer) as well as by GC-MS (Bruker EVOQ GC-TQ) (Fig. ESI-1-3). In the case of $Fu(Me)_2$, due to the difficulties in its synthesis and isolation, the used response factor for its quantification was that estimated for FuMe, considering the high degree of similarity between both molecules. The compound was also confirmed by GC-MS (Fig. ESI-4). Catalytic results are shown either in terms of conversion of furfural (X_{FUR}) or in terms of yield/selectivity towards the condensation adducts shown in Scheme 1 (Y_i/S_i respectively). The following definitions apply:

$$X_{FUR} = \frac{(\text{initial mmol of furfural}) - (\text{final mmol of furfural})}{\text{initial mmol of furfural}} \text{ x } 100 \quad (1)$$

$$Y_i = \frac{\text{mmol of product i}}{\text{initial mmol of furfural}} \text{ x } 100 \quad (2)$$

$$S_i = \frac{Y_i}{X_{FAL}} \text{ x } 100 \quad (3)$$

3. Results and Discussion

3.1 Catalysts screening

Commercial catalysts

Acid and base catalysts can catalyze the reaction of aldol condensation of ketones and aldehydes. Hence, we first tested several commercial acid/basic heterogeneous catalysts in order to evaluate the specific necessities of the transformation involving furfural (FUR) and methyl isobutyl ketone (MIBK). Table 1 summarizes the catalytic results in terms of conversion of FUR as the limiting reactant, as well as the selectivity of the reaction to the main condensation product (FuMe) over such commercial catalysts. It should be pointed out that, under the relatively mild reactions conditions chosen for this screening especially in terms of temperature, the formation of $Fu(Me)_2$ was not observed for most of the catalysts. Only the most active, calcium oxide, provided a negligible 0.4 % yield to $Fu(Me)_2$.

Table 1. Properties and catalytic performance of reference solid catalysts.

Catalyst	Type	Porosity (S_{BET})[a]	Acid/Base properties	Catalytic results[b] (%)	
				X_{FUR} (%)	S_{FuMe} (%)
Amberlyst-15	Cationic-exchange resin (sulfonic acid)	Macroporous (25)	Acid (Brønsted) 4.8 meq$H^+ \cdot g^{-1}$	55.4	19.3
H-Beta	Acid zeolite (BEA)	Microporous (623)	Acid (Lewis/Brønsted) Si/Al = 19	45.0	16.4
H-USY	Acid zeolite (FAU)	Microporous (680)	Acid (Lewis/Brønsted) Si/Al = 8.4	16.9	37.5
CaO	Alkaline earth metal oxide	Non-porous (5)	Basic	93.5	>99
ZrO_2	Transition metal oxide	Non-porous (4)	Amphoteric	57.6	8.1

[a] Surface area in $m^2 \cdot g^{-1}$ as provided by the supplier or experimentally determined. [b] Conversion of furfural (X_{FUR}) and selectivity to FuMe (S_{FuMe}); reaction conditions: 130 °C, reaction time 6 h, MIBK:FUR molar ratio 4:1, FUR:Cat mass ratio 5:1.

As shown, purely acidic catalysts generally lead to low selectivities towards the condensation adduct. The sulfonic resin Amberlyst-15, displaying strong Brønsted acid sites, leads to a high conversion of furfural but also to low selectivity, in a similar way to that provided by H-Beta zeolite (with aluminum-based Brønsted/Lewis acidity). H-USY, though providing better selectivity, shows the lowest conversion. It must be noted that furfural is a very reactive molecule in the presence of acid catalysts at high temperature, easily undergoing polymerization to form resinous species, which typically deposit on the catalysts surface and lead to catalyst deactivation by fouling. Hence, we hypothesize this as the main cause for the limited catalytic performance of such acid solids. In contrast, calcium oxide displays very high conversion accompanied by 100% selectivity, evidencing that strong basic sites are able to drive the aldol condensation of FUR and MIBK in a very efficient and selective way. Indeed, alkaline earth metal oxides and hydrotalcites have been regarded as potential heterogeneous catalysts for industrial application in aldol-condensation reactions, due to their strong basicity and low cost (especially in the case of CaO). However, technical concerns relative to the instability of this type of oxides upon exposure to moisture and CO_2 in air, as well as to water molecules in reaction,[39] have prevented them to reach the industrial scene in a broader way. Nonetheless, efforts are being taken towards the stability enhancement of such heterogeneous base catalysts.[40] On the other hand, zirconium oxide, usually considered as an amphoteric solid which exhibits both anion- and cation-exchange properties depending on the solution pH and the nature of the buffer,[41] is able to convert furfural but the formation of FuMe is very low. This poor result can be attributed, at least in part, to the low surface area of this solid, though the distribution and intensity of basic sites in this amphoteric solid is also an important parameter to take into account.

Zr-based synthesized catalysts

The previous results prompted us to test other heterogeneous catalysts, trying to replicate the excellent catalytic behavior of heterogeneous strong bases but with improved stability. In this sense, Zr-based materials have attracted much attention for the valorization of biomass as promising candidates, with versatile catalytic properties and high stability in organic reaction media. Thus, and taking advantage of our experience with Zr-based materials in different biomass valorization approaches during the last decade, we performed a complete screening including the following synthesized porous materials: Zr-modified Beta and USY zeolites; Zr-functionalized SBA-15; zirconia-coated SBA-15; Zr-based UiO66 MOFs. Table 2 and Fig. ESI-5-6 gather the most relevant physicochemical properties of these materials, whereas Fig. 1 depicts their catalytic performance in the aldol condensation of FUR and MIBK.

Table 2. Physicochemical properties of Zr-based synthesized catalysts.

Catalyst	Type	Zr (%wt)[a]	Al (%wt)[a]	BET area ($m^2 \cdot g^{-1}$)[b]	V_p[c] ($cm^3 \cdot g^{-1}$)	D_p[d] (Å)
UiO-66(Zr)	MOF	39.5	-	1080	1.05	5-10
UiO-66(Zr)-FA	Formic acid-modulated MOF	35.6	-	1658	0.80	5-20
ZrO_2-SBA-15	Mesostructured silica	17.0	-	367	0.75	83
Zr-SBA-15	Mesostructured silica	8.4	-	533	1.26	123
Zr-Beta(0.0)	Zeolite (BEA structure)	5.2	0.04	520	0.32	5.6-7.7
Zr-Beta(0.5)	Zeolite (BEA structure)	3.8	0.60	570	0.33	5.6-7.7
Zr-Beta(1.4)	Zeolite (BEA structure)	2.7	1.10	560	0.31	5.6-7.7
Zr-USY	Zeolite (FAU structure)	10.5	0.33	864	0.61	7.4

[a] Zr and Al contents measured by ICP-OES (in the case of MOF samples Zr content was estimated from TGA residue). [b] Total surface area calculated by the BET method from the adsorption branch of the corresponding nitrogen/argon isotherm. [c] Total pore volume recorded at P/Po = 0.975. [d] Mean pore size, for the zeolites corresponding to the respective crystalline topology.

Regarding the Zr-modified zeolites, herein prepared via a post-synthetic incorporation of the Zr species after removal of aluminum, the synthesized materials display a notable improvement in the selectivity to FuMe in comparison to the original H-Beta and H-USY commercial samples (Table 1). In the series of Zr-Beta materials, decreasing the ratio Al/Zr allows to make more selective the aldol condensation, achieving a maximum of 82% S_{FuMe} for the most dealuminated sample, Zr-Beta(0.0). However, the activity of the materials (X_{FUR}) drops to 20-25% (from 45% in H-Beta). As we have previously reported, the reduction of the Al/Zr ratio in these materials directly correlates with a reduction in the Brønsted/Lewis acid sites ratio.[37] Therefore, down-regulating the B/L ratio in these samples helps to increase the selectivity, most likely because of an increasing prevention of the acid-catalyzed non-desired side reactions of furfural. The limited conversion of FUR can be partially attributed to the limited pore diameter of the Beta zeolites, especially considering the formation of a relatively bulky molecule such as FuMe. On the other hand, for USY zeolite the behavior is different. Here, the

incorporation of Zr leads to a remarkable increase of X_{FUR} relative to H-USY zeolite, whereas the selectivity remains in a similar level. This seems to indicate that H-USY material undergoes a fast deactivation limiting its conversion, because of the higher Al content and acid strength in this zeolite. After dealumination and subsequent modification with Zr, such effect is minimized and the conversion can reach higher values. The larger pores of FAU structure (Zr-USY) vs. BEA structure (Zr-Beta), together with the higher Zr loading, might be the explanation for the enhanced X_{FUR} in the former. However, the selectivity remains below 45% (Fig. 1).

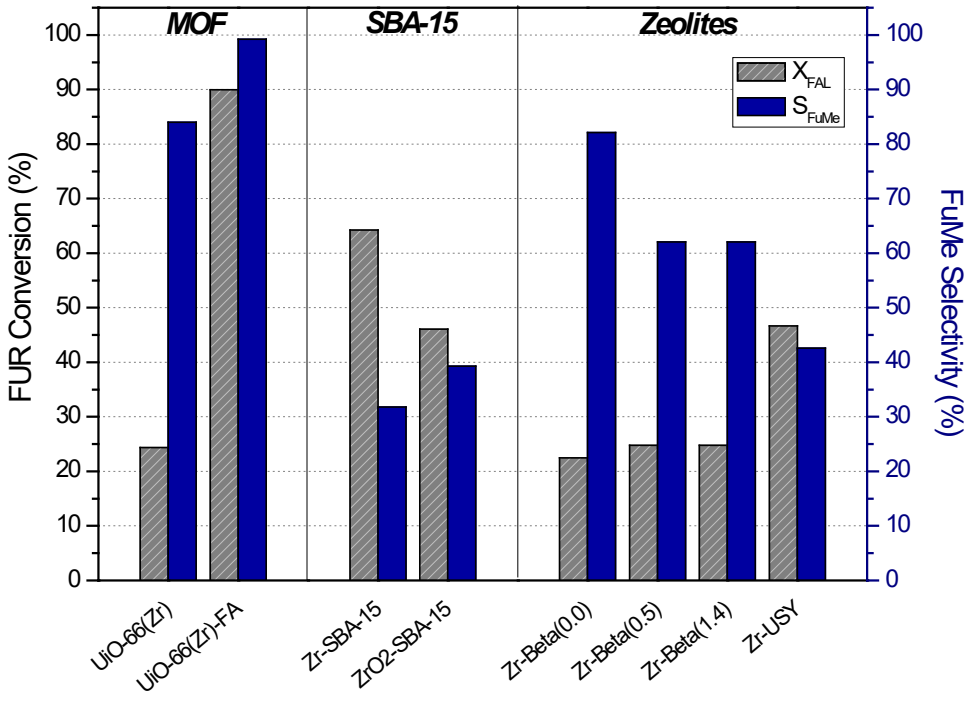

Figure 1. Conversion of furfural (X_{FUR}) and selectivity to FuMe (S_{FuMe}) over Zr-based synthesized catalysts; reaction conditions: 130 °C, 6 h, MIBK:FUR ratio (mol/mol) 4:1, FUR:Cat ratio (wt/wt) 5:1.

Both Zr-based SBA-15 samples display the high surface area and mesopores uniform size typical of SBA-15 mesostructured materials (Table 2, Fig. ESI-6). In Zr-SBA-15 catalyst, where isolated Zr species are evenly incorporated within the silica mesostructure, a moderate Brønsted acidity has been attributed to surface silanols, with the Zr providing Lewis acidity.[36] In turn, ZrO_2-SBA-15 displays a thickness-controlled zirconia coating grown from the silica walls of a previously synthesized SBA-15 material. This strategy allows obtaining a highly dispersed and accessible silica-grafted thin layer of zirconium oxide, containing two Zr species, those at the interface with silica and those within tetragonal ZrO_2 crystallites associated with strong and weak Lewis acid sites respectively.[42] Both catalysts have proven to be good candidates for other biomass transformations where modulation of acid and textural properties is critical. Here, in the aldol condensation

of FUR with MIBK, they are both relatively active, but the selectivity to FuMe remains below 40% (Fig. 1). Although they perform better than the commercial acid catalysts, especially much better than their related ZrO_2 reference (Table 1), they are still far from the highly efficient CaO material.

Next, we tested the synthesized Zr-based MOF catalysts in reaction. These materials, unlike the previous ones, are characterized by the organic nature of the matrix linking together the Zr clusters, as well as by excellent textural properties and high content of Zr (Table 2). Thus, standard UiO-66(Zr) consists of hexanuclear, octahedral zirconium oxoclusters connected through terephthalate (1,4-benzenedicarboxylate) linkers to form the rigid 3D-framework with a high degree of topological connectivity (ideally 12-coordination in the metal center). In the case of UiO-66(Zr)-FA, the use of formic acid (FA) as modulator during the synthesis has been reported to interfere on the formation of the structure, eventually leading to the creation of defects in the crystalline structure.[33,43] Fig. 1 shows that UiO-66(Zr) provides poor FUR conversion (24%), though the selectivity to FuMe (84%) is higher than in the case of zeolites and mesostructured materials. However, the use of FA as modulator clearly boosts the catalytic performance, reaching outstanding values of X_{FUR} (90%) and S_{FuMe} (>99%), in the same order than that displayed by CaO. This would be a clear example of the beneficial effects of introducing defects in the MOF 3D-scaffold to improve the catalytic properties in this kind of materials. Noteworthy, as in the case of the acid-base catalysts included in Table 1, the Zr-based catalysts of this screening did not provide $Fu(Me)_2$ as a further condensation product due to the relatively mild reactions conditions used. The exception is the highly active UiO-66(Zr)-FA, that yielded 0.8% of $Fu(Me)_2$.

In order to get a better insight of the underlying reasons of such an improvement in catalysis of the Zr-based MOF, both materials were further characterized at the microscopic level. Fig. 2 includes the XRD diffractograms and the N_2 adsorption-desorption isotherms. The overall framework structure of UiO-66 is virtually unchanged after introduction of defects through modulation with formic acid, as seen by powder XRD (Fig. 2a). It must be noted that the ability to maintain the network structure upon dehydroxylation and change in coordination around Zr is inherent to the structural stability of this family of MOFs.[28] In the UiO structure, access to the internal surface of Zr-MOFs is restricted by triangular windows, being estimated the opening thereof from the largest sphere that may fit the window. Terephthalate linkers used in UiO-66 MOF, displaying only one benzene ring in contrast to those of UiO-67 (two benzenes) or UiO-68 (three benzenes), ideally result in pore openings around 6-10 Å.[28] Thus, we hypothesize that a relatively bulky molecule such as FuMe –and especially $Fu(Me)_2$– will likely suffer from steric hindrances within the UiO-66(Zr) structure, leading to the limited catalytic performance observed over UiO-66(Zr) (Fig. 1). Indeed, the estimated kinetic diameters for FuMe and $Fu(Me)_2$ are approximately 7.1 and 8.4 Å, respectively, as determined by using the critical properties thereof following the procedure reported by Huber et al [44]. For the calculation of the respective critical properties (T_c, P_c and V_c), a group-contribution based estimation of pure component properties has been applied (Joback-Reid method [45]). Therefore, the diffusion of such molecules would be partially hindered in

the pore size range of 6-10 Å displayed by the non-modified UiO-66(Zr) catalyst. Consequently, a controlled introduction of defects via modulation with FA during the synthesis would help in facilitating access for the bulkier products to, and from, the Zr active sites in a much larger extent. This is confirmed by the higher BET surface area in the modified UiO-66(Zr)-FA material (Table 2), and by the clear variation in the argon adsorption isotherm (Fig. 2b, insert). Likewise, in UiO-66(Zr)-FA material, the pore size distribution shows the formation of a secondary porosity in the range of 15-20 Å (with a remaining contribution from pores in the range of 6-7 Å), which would be much more suitable for the management of molecules of the size of the condensation adducts. This new larger pores, not present in UiO-66(Zr), can be attributed to missing-node (Zr_6O_8 clusters) defects, as these defects are associated with larger pores than missing-linker defects, which have been reported to be favored by acid modulators.[43] However, it must be noted that missing-node and missing-linker defects may co-exist within the same material, as carboxylic acids like FA can yield both.

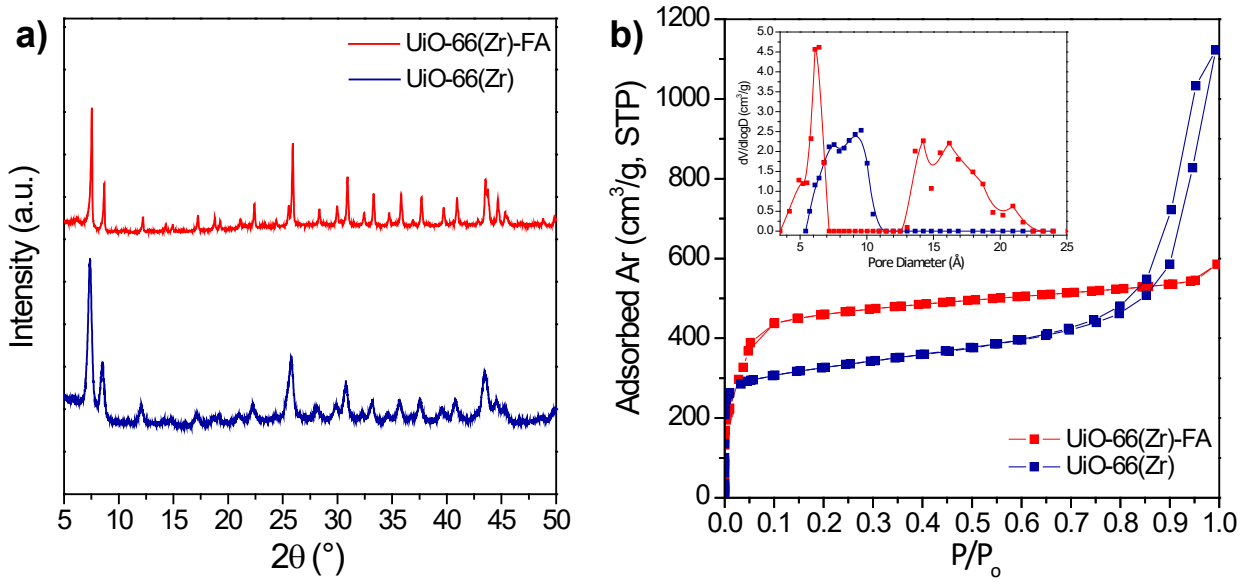

Figure 2. a) Powder X-Ray Diffraction patterns, b) Argon adsorption-desorption isotherms and pore size distributions corresponding to UiO-66(Zr) and UiO-66(Zr)-FA catalysts.

TGA performed on both samples (Fig. ESI-7) also evidences the introduction of missing-node defects in UiO-66(Zr)-FA, as the total organic content increases from 46.5% to 51.9%. Accordingly, the Zr content, determined from the residual ZrO_2 at 900 °C in the thermogravimetric analysis, decreases from 39.5% to 35.6% (Table 2). This serves to corroborate that the missing-node defects are more significant than the missing-linker defects. To assess the atom-environment variations, Zr and O environments in the UiO-66 materials were further characterized by means of X-ray photoelectron spectroscopy (XPS). Zr 3d XPS spectra (Fig. 3-left) reveal a small shift of both Zr 3d signals (5/2 and 3/2) to higher binding energies in the FA-modulated sample, indicating a

change of the Zr environment. As a reference, Zr 3d XPS spectrum corresponding to crystalline zirconium oxide[46] is much closer to the spectrum of UiO-66(Zr) than to that of UiO-66(Zr)-FA, which would be in agreement with the partial substitution of terephthalate linkers in close proximity to Zr atoms. A similar behavior has been previously reported in hierarchical Zr-based UiO-66 materials with defects.[47] XPS spectra for O 1s (Fig. 3-right) also evidence the differences between both materials. Three peaks centered at binding energies 533.3, 531.9 and 530.5 eV can be observed in the O 1s spectra. These peaks can be assigned to the oxygen atoms in carboxylate groups (O-C=O), Zr-O-C moieties and bridging linked (η^3-O-Zr_3) groups, respectively.[47] In the FA-modulated sample, a reduction in the population of carboxylate oxygen atoms (from non-fully coordinated terephthalic linker groups), as well as an increasing of Zr-O-Zr motifs (oxygen in the Zr oxo-clusters constituting the nodes of the framework, i.e. μ_3-O and μ_3-OH species) can be observed. This is consistent with the introduction of defects in UiO-66(Zr)-FA material.

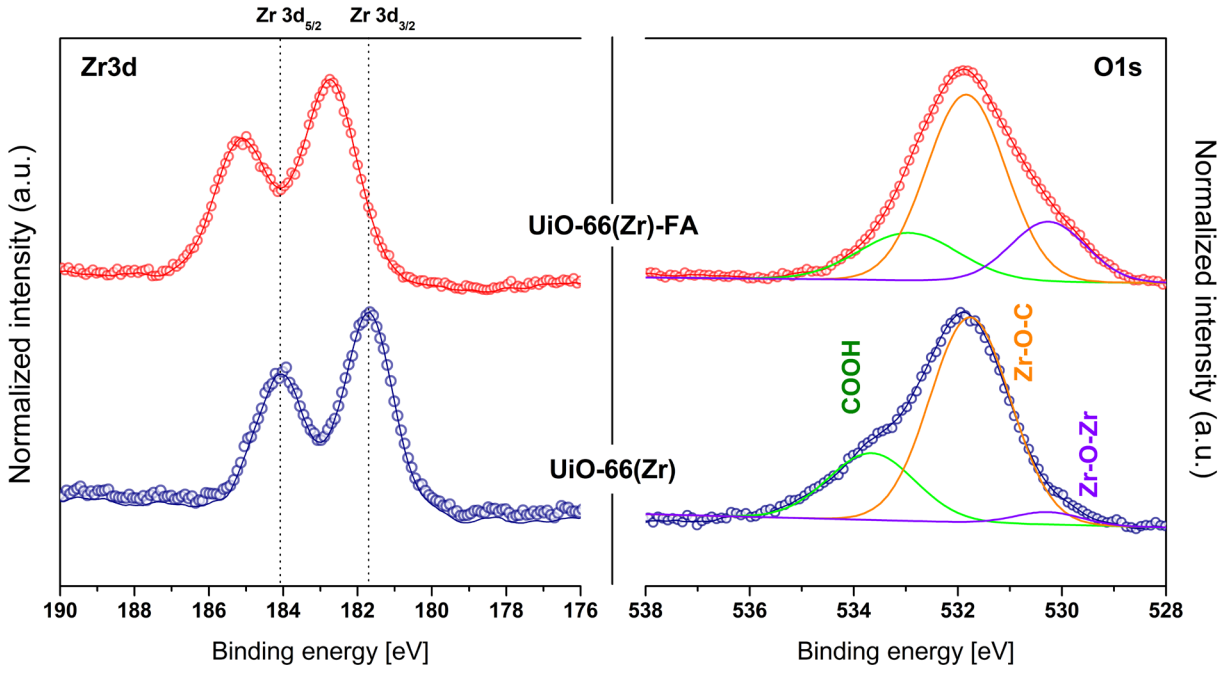

Figure 3. High-resolution Zr 3d (left) and O 1s (right) XPS spectra, of UiO-66(Zr) and UiO-66(Zr)-FA catalysts.

Regarding the acid/base properties of UiO-66 materials, it has been reported that missing-linker defects, as those above-discussed, confer weak Brønsted acidity due to the increased availability of structural μ_3-OH hydroxyl groups belonging to the Zr_6 cluster. Indeed, acid-base titration experiments carried out following a previously reported procedure,[48] confirmed the increase in acidity corresponding to μ_3-OH moieties, from 1.47 meq/g to 3.05 meq/g (Fig. ESI-8). We also performed DRIFT using deuterated acetonitrile as molecular probe on both MOF materials. Deuterated acetonitrile has been found to be a suitable molecule for

differentiating among acid sites of different strengths.[49] The analysis of the desorption kinetics (Fig. ESI-9) allowed establishing the evacuation conditions at 50 °C for 5 min to remove any residual physisorbed CD_3CN. Fig. 4 includes the resulting spectra obtained on UiO-66 samples within the region of 2400-2200 cm^{-1}, with and without applying a previous drying step at 120 °C to remove any interfering physisorbed water molecules. In this analysis, Brønsted acid sites can be sorted by their strength showing different wavelengths in the 2300-2270 cm^{-1} range in the infrared spectrum. IR peaks detected approximately at 2295 cm^{-1}, 2277 cm^{-1} and 2270 cm^{-1}, are typically associated with the stretching of the bound C≡N group attributed to strong, medium, and weak Brønsted acid sites, respectively. The region corresponding to Lewis acid sites spreads to larger wavenumbers (2340-2300 cm^{-1}), however the acquired spectra did not show any significant signals for any of the materials in this region, either dried or non-dried, under the experimental conditions tested. The UiO-66(Zr)-FA material is sensitive to the drying process (5-fold increase in recorded intensity), and the presence of acidity can be observed. We identified a broad Brønsted acidity contribution, not very strong, at 2266-2277 cm^{-1} (Fig. 4), which can be attributed to an increase of available μ_3-OH hydroxyl groups because of the introduced defects in the MOF structure. This assignment is in accordance with the titration and XPS techniques. On the contrary, the non-modulated UiO-66(Zr) MOF does not show relevant acid properties under molecular probing. Indeed, the recorded band intensity is very low and weak, wavenumber at 2266 cm^{-1}, and does not show differences between the dried and non-dried samples. This might be attributed to a lack of accessibility to the acid sites. On the other hand, Chakarova et al have recently proposed also the existence of a hidden Lewis acidity coming from Zr^{4+} Lewis acid sites.[50] They reported that evacuating the materials at high temperature (200 °C or higher), yields an unambiguous infrared band at 2300 cm^{-1} for CD_3CN, explained by a structural re-arrangement of the Zr^{4+} environment induced by relatively strong bases like CD_3CN. However, temperatures above 200 °C may affect the structural integrity of the MOF and this conclusion should be considered carefully when extrapolated to the behaviour under milder reaction conditions, as those used in the present work. Additionally, in the condensation of FUR and MIBK, water molecules are released to the reaction media as a by-product, favouring a more Brønsted-type in-situ behaviour of the catalytically active sites.

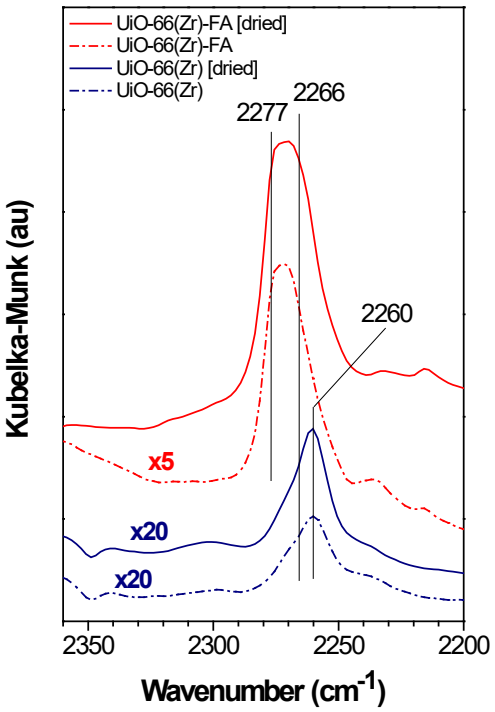

Figure 4. DRIFT spectra obtained for adsorbed CD_3CN on UiO-66(Zr) and UiO-66(Zr)-FA catalysts, before and after drying at 120 °C.

In conclusion, we attribute the catalytic activity of these materials mainly to the activity of the μ_3-OH hydroxyls within the zirconium clusters. Such hydroxyl groups are the most numerous acid groups in this kind of MOFs, being considered Brønsted in nature. [51] Noteworthy, the active sites for this type of aldol condensation (when acid-catalysed) are reported to be mainly the Brønsted acid sites. Indeed, Brønsted acidity arising from defects and rehydration in MOF materials has been ascribed as the main responsible for catalysing the aldol condensation of furfural and acetone, whereas the Lewis acidity of MOFs is not enabling such transformation. [52] Therefore, the preferential active sites to perform the acid-catalysed aldol condensation of furfural and MIBK would be the Brønsted acid sites. However, it is well know that such Brønsted acid sites can also catalyse the undesired size reactions of furfural, especially when they present high acid strength. This is the case, e.g., of the sulfonic acid resin Amberlyst-15 or the acid zeolites (Table 1), which present strong Brønsted acid sites leading to low selectivity for the aldol condensation. In turn, the Brønsted acidity in the UiO-66(Zr) materials, coming from the μ_3-OH groups, is of weak strength. This prevents the occurrence of furfural side reactions like oligo- and polymerization, allowing for much higher selectivity to the aldol condensation. The weak acid strength of such hydroxyl groups is herein confirmed through the DRIFT experiments using CD_3CN as basic probe.

3.2 Analysis of kinetics and reaction conditions for the aldol condensation of FUR and MIBK over UiO-66(Zr)-FA

To improve the understanding of the reaction system, aiming to identify the conditions leading to non-desired by-products, a pseudo-homogeneous kinetic model has been applied. In this way, we evaluated the kinetics of the reaction varying the temperature in the range 110-170 °C, using a FUR/Cat mass ratio = 10. For this experiment, the ratio MIBK/FUR (mol/mol) was fixed at 4 from a previous study (Fig. ESI-10), aiming to avoid limitations in the catalytic process due to a low availability of the ketone in the reaction media. Scheme 2 describes the proposed simplified reaction pathway with the apparent rate constants for each step. The process starts with the aldol condensation of FUR with MIBK (reaction step #1, k_1). Then, the so-formed adduct (FuMe) may undergo a second condensation reaction with another molecule of MIBK to produce $Fu(Me)_2$ (reaction step #2, k_2). The formation of degradation compounds, herein lumped as 'humins', has been considered to occur mainly from FuMe (reaction step #3, k_3). Indeed, in view of the experimental results, the formation of humins from FUR is very low when using UiO-66(Zr)-FA as catalyst, since its transformation into FuMe is fast and highly favored. Humins concentration was estimated as the difference between the identified products and the closure of the mass balance. For the sake of simplicity, first order pseudo-homogeneous kinetics has been assumed for the three steps involved in the process.

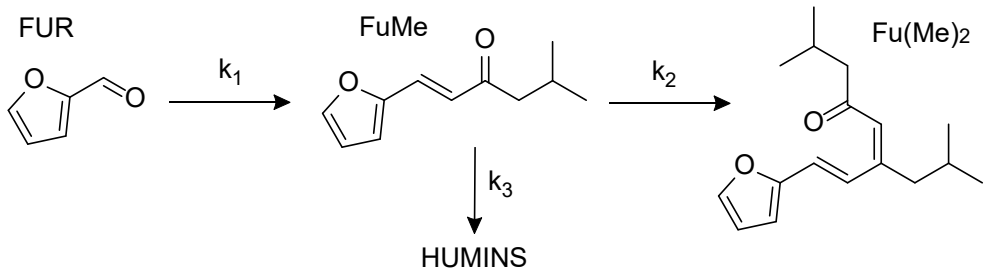

Scheme 2. Proposed reaction network for the aldol condensation of FUR and MIBK. Humins: degradation products.

Thus, for the reaction network considered, the model equations are as follows:

$$\frac{dC_{FUR}}{dt} = -k_1 \cdot C_{FUR}$$

$$\frac{dC_{FuMe}}{dt} = k_1 \cdot C_{FUR} - k_2 \cdot C_{FuMe} - k_3 \cdot C_{FuMe}$$

$$\frac{dC_{Fu(Me)2}}{dt} = k_2 \cdot C_{FuMe}$$

$$\frac{dC_{Humins}}{dt} = k_3 \cdot C_{FuMe}$$

Where C is the molar concentration of each component, and k_i is the apparent rate constant corresponding to step # *i* at a constant temperature. The differential equations system was solved by numerical integration and simultaneous optimization, using the tool Microsoft® Excel SOLVER, by minimizing the objective function defined as the sum of the residual squares:

$$F_{obj} = \sum_{m} \left\{ \sum_{n=1}^{n_p} \left[C_{m,n,calc} - C_{m,n,exp} \right]^2 \right\}$$

where $C_{m,n,calc}$ and $C_{m,n,exp}$ are the calculated and experimental concentrations of component *m* (FUR, FuMe, $Fu(Me)_2$ and Humins) at reaction time *n*, respectively. Likewise, an Arrhenius analysis was applied to get the activation energy of each reaction step. Table 3 displays the resultant kinetic parameters of the modelled transformation. Experimental and modelled concentrations of each compound involved in the process of aldol condensation of FUR and MIBK over UiO-66(Zr)-FA are depicted together in Fig. 5, evidencing the good agreement between the experimental data and the model-predicted values.

Table 3. Apparent rate constants (k_i), activation energies (E_a) and pre-exponential factors (k_0), and Arrhenius analysis of the modelled aldol condensation of FUR and MIBK over UiO-66(Zr)-FA in the temperature range 110-170 °C.

Reaction step #	k_i (h^{-1})				E_a ($kJ \cdot mol^{-1}$)	k_0 (h^{-1})	R^2
	110 °C	130 °C	150 °C	170 °C			
1	0.0896	0.3655	1.1438	2.0993	75.28	1.86×10^9	0.98
2	0.0000	0.0000	0.0575	0.1232	59.40	1.24×10^6	1.00
3	0.0000	0.0000	0.0306	0.0686	62.98	1.82×10^6	1.00

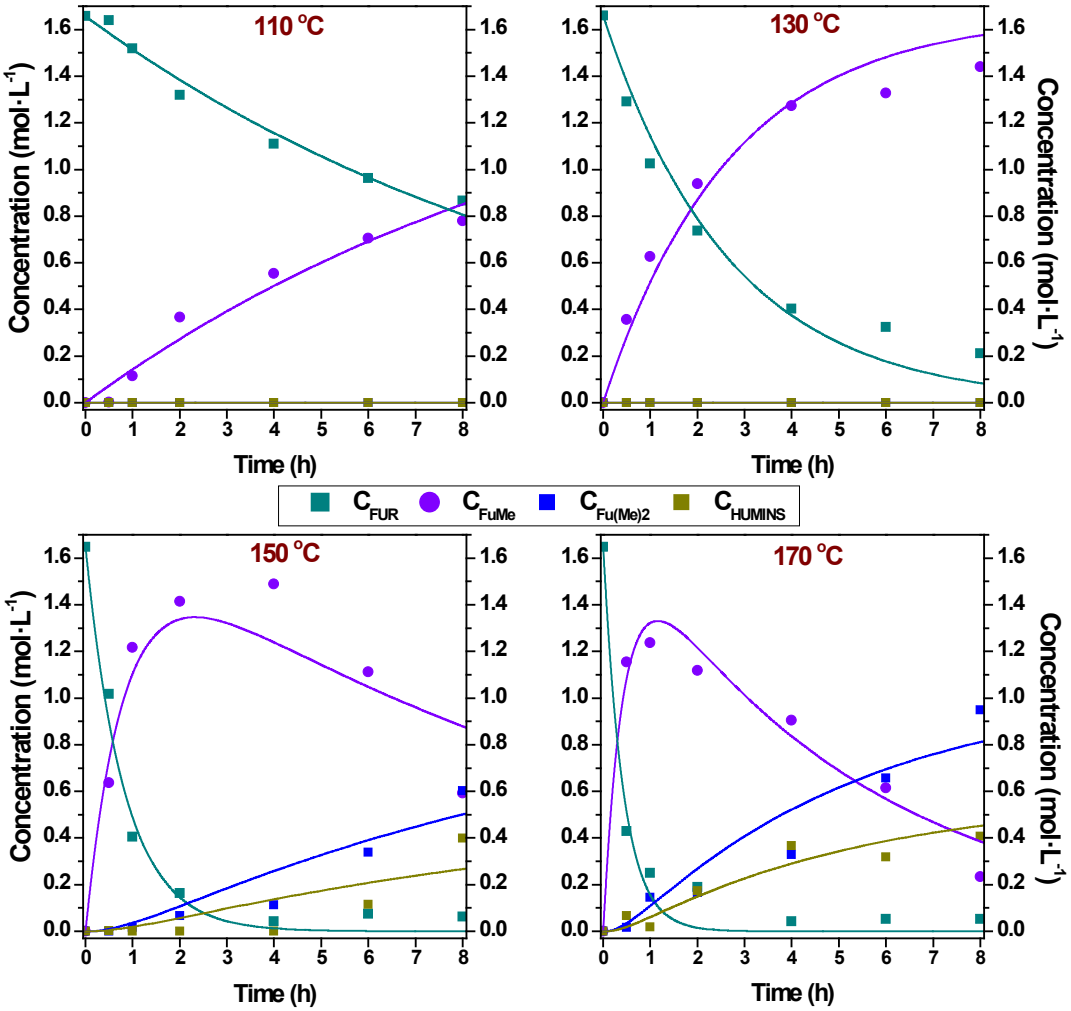

Figure 5. Experimental (symbols) and modelled (solid lines) concentration of the compounds involved in the process of aldol condensation of furfural and MIBK over UiO-66(Zr)-FA. Reaction conditions: temperature range = 110-170 °C; FUR/Cat mass ratio = 10; MIBK/FUR molar ratio = 4.

The analysis of the apparent kinetic parameters calculated for each step allows establishing a comparison of the catalytic activity of the defective UiO-66(Zr)-FA in each reaction step involved in the process. The aldol condensation of starting FUR with MIBK to produce FuMe (step 1) present the highest kinetic constant, being the predominant transformation, and even the only one at low and moderate temperature (110-130 °C). In fact, the negligible values of the kinetic constants obtained for reaction steps 2 and 3 at the lower temperatures confirm the scarce formation of by-products under these conditions. On the other hand, the formation of the higher adduct, $Fu(Me)_2$, requires of higher temperature to take place. However, the increase in the temperature to ≥ 150 °C unavoidably leads to the concomitant formation of the non-desired *humin*-type compounds. Thus, despite the

conversion of FUR at the highest temperature (170 °C) is very fast, reaction steps 2 and 3 also become relevant making impossible to reach a total selectivity to FuMe.

On the other hand, to assess the most influential variables as well as the existence of possible interactions among them a factorial design and the response surface methodology were followed.[53] A full factorial face-centered composite design matrix of two variables (two factors and three levels for each one) was used to set the experimental design up. Temperature, as evidenced by the previous kinetics analysis, and furfural/catalyst mass ratio were selected as experimental factors due to their high influence of the catalytic performance. The levels chosen for temperature were 130, 150, and 170 °C, whereas the levels for the FUR/catalyst ratio were 2, 6, and 10 (wt/wt), and the catalytic runs were carried out at 4h. As response variables, the FUR conversion (X_{FUR}), and the selectivity to the aldol adduct (S_{FuMe}) were selected taking into account the main objective of achieving high conversion of FUR and high yield to FuMe, while minimizing the formation of undesired by-products. Table 4 includes the standard experimental matrix for the design. Second and third columns represent the factor levels on a natural scale, whereas fourth and fifth columns represent the 0 and ±1 encoded factor levels on a dimensionless scale. The central point experiment, corresponding to (0,0) in coded factors, was replicated four times (Runs # 1-4 in Table 4) in order to determine the variability of the results and assess the experimental error. Experiments were carried out at random to minimize the effect of possible systematic trends in the observed responses. The table also includes the experimental results of the response variables.

Table 4. Full factorial face-centered composite design matrix of two variables and the observed responses after 4 h of reaction in the optimization of FuMe production over UiO-66(Zr)-FA.

Run	Experimental factors				Response variables	
	T (°C)	FUR/Cat (wt)	X_1[a]	X_2[b]	X_{FUR}[c]	S_{FuMe}[d]
1	150	6	0	0	98.8	74.4
2	150	6	0	0	99.2	75.4
3	150	6	0	0	98.9	71.9
4	150	6	0	0	99.1	71.1
5	130	2	-1	-1	99.4	100.0
6	130	6	-1	0	89.4	100.0
7	130	10	-1	1	75.9	100.0
8	170	2	1	-1	98.9	4.9
9	170	6	1	0	98.1	11.1
10	170	10	1	1	98.3	33.3
11	150	2	0	-1	99.3	34.6
12	150	10	0	1	97.9	94.8

[a] Coded temperature; [b] Coded FUR/Cat; [c] Conversion of furfural (%). [d] Selectivity to FuMe (%). Other reaction conditions: time 4h, MIBK/FUR molar ratio 4/1.

The following predictive equations for conversion (Eq.1) and selectivity (Eq.2) were obtained by multiple regression analysis from the generated matrix of experimental data, and assuming a second-order polynomial model. An analysis of variance (ANOVA) was performed to calculate the regression coefficients. The following equations represent the statistical models obtained from encoded levels in a dimensionless scale from -1 to +1, providing the real influence of each variable on the process. To facilitate the interpretation of the equations, Fig. ESI-11 plots the response surfaces and contour plots of FUR conversion FuMe selectivity.

$$X_{FUR}(\%) = 99.02 + 5.1 \cdot X_1 - 4.25 \cdot X_2 - 5.35 \cdot X_1^2 + 5.73 \cdot X_1 \cdot X_2 - 0.5 \cdot X_2^2 \quad (r^2=0.925) \quad \text{Eq.1}$$

$$S_{FuMe}(\%) = 71.12 - 41.8 \cdot X_1 + 14.78 \cdot X_2 - 11.41 \cdot X_1^2 + 7.13 \cdot X_1 \cdot X_2 - 2.26 \cdot X_2^2 \quad (r^2=0.937) \quad \text{Eq.2}$$

Validation of the prediction capability of the models was performed by an evaluation of the regression error. The relatively high values recorded for the regression coefficients (r^2) are an indication of the goodness of the fit, which can be additionally visualized in the representation of experimental and predicted values (Fig. ESI-12). Furthermore, reproducibility of the experimental system is elevated, as evidenced by the arithmetical averages and standard deviations calculated from the central-point replicas (Runs #1-4, Table 3): FUR conversion (99.0 ± 0.2%), FuMe selectivity (73.2 ± 2.0%). The standard deviations were 0.2 and 2.0%, respectively, indicating a high reproducibility of the system.

For the analysis statistical significance (ANOVA) of each variable, a total error criteria with a confidence level of 95.0% was used. Thus, the significance of each parameter included in the models can be assessed from its P-value. Fig. ESI-13 shows the standardized Pareto chart for FUR conversion and FuMe selectivity over UiO-66(Zr)-FA catalyst, evidencing the significant and non-significant factors, as well as the positive or negative interactions. In this way, the statistical analysis in the studied experimental range identifies the temperature and the interaction temperature-FUR/Cat ratio as the most significant terms in the model in the FUR conversion response (Fig. ESI-13a). Both have a positive effect, meaning that an enhancement of the temperature by itself, but especially when accompanied by an increase of the FUR/Cat ratio, leads to an increase in the conversion of FUR. In contrast, FUR/Cat ratio by itself and the quadratic effect of the temperature display a significant negative influence on the conversion, because of the curvature effect observed at high values of both variables. In the case of the selectivity to FuMe (eq.2, Fig. ESI-13b), the temperature is identified as the most –and almost only– significant factor, having an overall negative effect on this response. Additionally, the linear effect of the FUR/Cat ratio shows a small but significant effect on the S_{FuMe}. This results in the absence of curvature for this model, leading to the maximum values of selectivity (close to 100%) at the lowest temperature and at the highest FUR/Cat ratio. However, the simultaneous maximization of X_{FUR} and S_{FuMe} is better attained at low FUR/Cat. According to the model, the predicted optimal conditions would be T = 130 °C y FUR/Cat = 2, which lead to X_{FUR} = 99.4 %; and S_{FUME} = 100%. In conclusion, from the point of view of a highly selective and active process, it appears necessary to operate at moderate

temperature, to keep high selectivity, while adequately adjusting the FUR/Cat ratio to low values, to reach high conversion.

3.3 Stability and reusability of UiO-66(Zr)-FA catalyst

In order to analyse the potential leaching of Zr species to the reaction medium, which would not only imply a deterioration of the catalyst but also provide a homogeneous contribution to the catalytic effect, a hot-filtration experiment was carried out. In this test, a typical catalytic run was set and the reaction initiated as usual. Then, at a given reaction time (herein 2h), the catalyst was removed from the reaction mixture by simple filtration, and the clear liquid mixture was returned to the reactor to continue with the process. Fig. 6 compares the results obtained from this catalyst-removed test with a normal one (without removing the catalyst). It demonstrates that the reaction does not continue progressing once the catalyst has been filtered off, so a homogeneous contribution to the observed catalytic effect from solubilized Zr species can be discarded. Likewise, the XRD diffraction pattern corresponding to the catalyst after three uses in reaction (Fig. ESI-14) evidences that the crystalline structure of the MOF material is preserved, indicating the high degree of stability of the UiO structure.

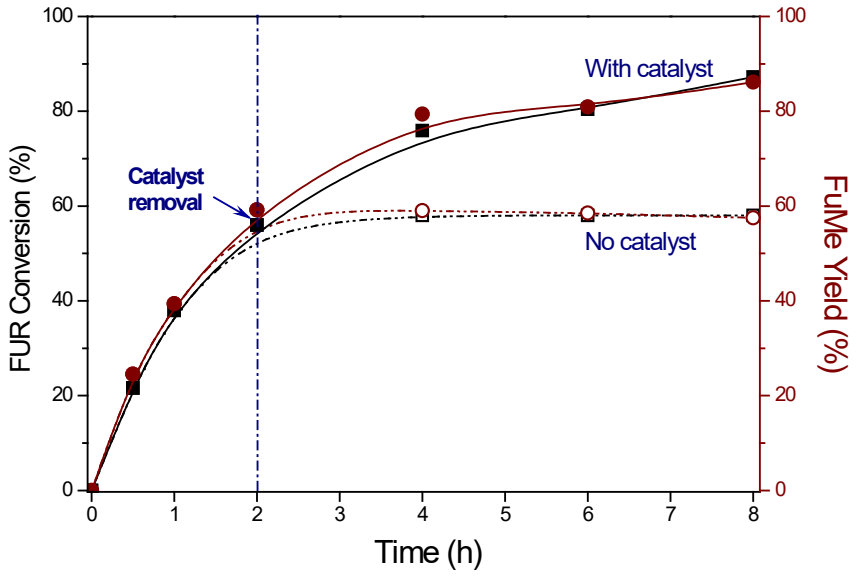

Figure 6. Hot filtration test of UiO-66(Zr)-FA. Catalyst was removed after 2h and the reaction was continued without catalyst (dashed line). For comparison purposes, the same reaction completed with catalyst is also included (solid line). Reaction conditions: temperature = 130 °C; FUR/Cat mass ratio = 10; MIBK/FUR molar ratio = 4.

On the other hand, the reusability of UiO-66(Zr)-FA was evaluated by reutilization experiments in six consecutive short 1h-reaction cycles to avoid complete conversion conditions that might lead to false conclusions. Likewise, as furfural is the main potential cause of catalyst deactivation, two levels of furfural concentration (FUR/Cat mass ratio = 2 and 10) were evaluated. After each run, the catalyst was recovered by filtration, rinsed with acetone and directly loaded into the reactor for the next catalytic run, without applying any regeneration treatment. Fig. 7 includes the results in terms of X_{FUR} and S_{FuMe}. As shown, under these more moderate reaction conditions, the first use of the UiO-66(Zr)-FA catalyst does not lead to total conversion (X_{FUR} = 90% and 38%, at FUR/Cat = 2 and 10, respectively). However, there is a clear and progressive deactivation effect after each new use of the catalyst evidenced by a decay in the conversion of furfural (though the selectivity to FuMe remains high). This is especially enhanced at the highest level of FUR/Cat ratio (10), indicating that the main cause for the deactivation in this system is intimately related to the presence of furfural at high concentration.

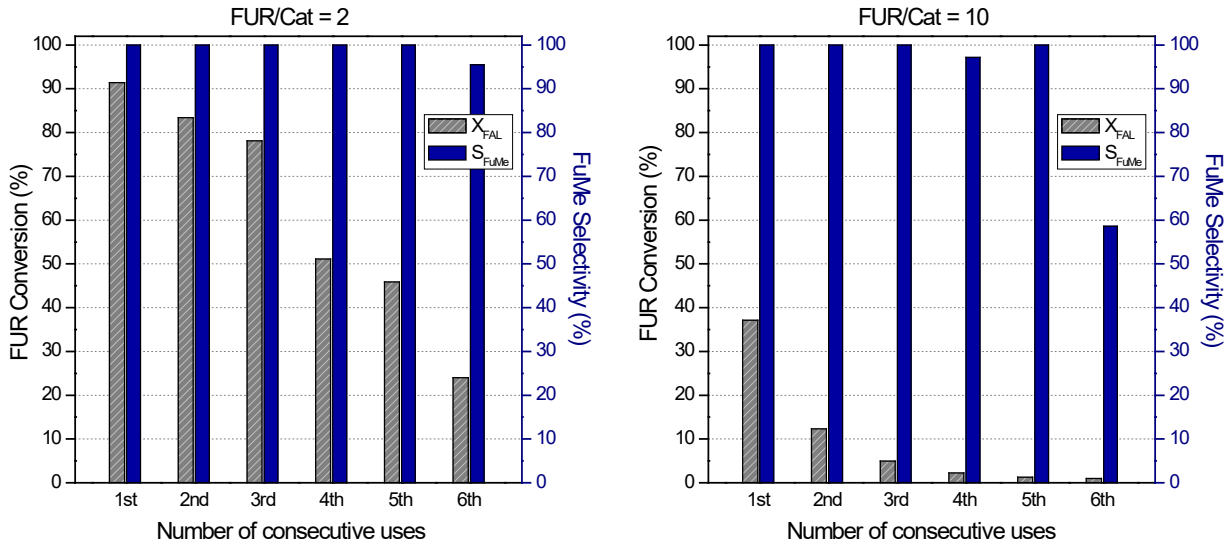

Figure 7. Reutilization of UiO-66(Zr)-FA in the aldol condensation of FUR and MIBK into FuMe at two levels of FUR/Cat mass ratio, 2 (left) and 10 (right). Reaction conditions: time = 1h; temperature = 130 °C; MIBK/FUR molar ratio = 4.

This prompted us to evaluate the status of the spent catalysts through some additional characterization. In this way, the catalysts were recovered after 6 reaction uses (for both FUR/Cat ratios) and the acidity was assessed again by means of acid-base titration. As shown if Fig. ESI-15, there is a clear reduction in the acid capacity related to the μ_3-OH active sites in both sets of reusing experiments, down to values of 1.30 and 1.27

meqH^+/g (from 3.05 meqH^+/g in the fresh material). Therefore, we attribute the activity decay to the blocking of the active sites by organic deposits coming from furfural side reactions.

4. Conclusions

This work addresses the preparation of defective UiO-66(Zr) by using formic acid as modulator during the synthesis and its application to catalyse the aldol condensation reaction of furfural and methyl isobutyl ketone (MIBK) for the production of jet-fuel precursor. Formic acid-modulated UiO-66(Zr) shows a remarked increase in the catalytic performance both in terms of furfural conversion and selectivity to the most interesting condensation product (FuMe), which is ascribed to the incorporation of defects to the material. In this way, the presence of ligand-missing and node-missing defects has been confirmed by different techniques, leading to an increase in the accessibility to the active sites, as confirmed by the structural and spectroscopic characterization. Thus, μ_3-OH hydroxyls of the Zr_6 clusters, of weak Brønsted acid nature, are made more available in the defective solid, being this the most plausible reason for the observed sharp increase in activity. Additionally, the analysis of the reaction kinetics, together with the optimization of the reaction conditions, identified the temperature as the most relevant parameter affecting the selectivity to FuMe. Thus, under the optimized reaction conditions (130 °C; 4 h; FUR/Cat = 2; MIBK/FUR = 4) total FUR conversion and FuMe selectivity (~100%) can be achieved. However, the catalyst is progressively deactivated in successive catalytic runs under the studied reaction conditions, in a manner strongly dependent on the furfural concentration. Such deactivation is thus attributed to the formation of organic deposits coming from furfural side reactions. Further study is still necessary to address the possible regeneration of the material.

Acknowledgements

Financial support from the Spanish Ministry of Science and Innovation, grant numbers RTI2018-094918-B-C42 and RTI2018-094918-B-C41; the Regional Government of Madrid, grant number P2018/EMT-4344; and University Rey Juan Carlos (Young Researchers R&D Project ref. M2181-BIOCAVI) is gratefully acknowledged.

References

[1] European Commission, Communication From the Commission to the European Parliament, the Council, the European Economic and Social Committee and the Committee of the Regions: The European Green Deal, Publications Office of the European Union, 2019.

[2] H. Wang, B. Yang, Q. Zhang, W. Zhu, Catalytic routes for the conversion of lignocellulosic biomass to aviation fuel range hydrocarbons, Renewable and Sustainable Energy Reviews. 120 (2020) 109612. https://doi.org/10.1016/j.rser.2019.109612.

[3] X. Han, Y. Guo, X. Liu, Q. Xia, Y. Wang, Catalytic conversion of lignocellulosic biomass into hydrocarbons: A mini review, Catalysis Today. 319 (2019) 2–13. https://doi.org/10.1016/j.cattod.2018.05.013.

[4] Y. Nakagawa, M. Tamura, K. Tomishige, Recent development of production technology of diesel- and jet-fuel-range hydrocarbons from inedible biomass, Fuel Processing Technology. 193 (2019) 404–422. https://doi.org/10.1016/j.fuproc.2019.05.028.

[5] H. Li, A. Riisager, S. Saravanamurugan, A. Pandey, R.S. Sangwan, S. Yang, R. Luque, Carbon-Increasing Catalytic Strategies for Upgrading Biomass into Energy-Intensive Fuels and Chemicals, ACS Catalysis. 8 (2018) 148–187. https://doi.org/10.1021/acscatal.7b02577.

[6] R. Gérardy, D.P. Debecker, J. Estager, P. Luis, J.-C.M. Monbaliu, Continuous Flow Upgrading of Selected C 2 –C 6 Platform Chemicals Derived from Biomass, Chemical Reviews. 120 (2020) 7219–7347. https://doi.org/10.1021/acs.chemrev.9b00846.

[7] G.W. Huber, J.N. Chheda, C.J. Barrett, J.A. Dumesic, Production of liquid alkanes by aqueous-phase processing of biomass-derived carbohydrates, Science. 308 (2005) 1446–1450. https://doi.org/10.1126/science.1111166.

[8] C.J. Barrett, J.N. Chheda, G.W. Huber, J.A. Dumesic, Single-reactor process for sequential aldol-condensation and hydrogenation of biomass-derived compounds in water, Applied Catalysis B: Environmental. 66 (2006) 111–118. https://doi.org/10.1016/j.apcatb.2006.03.001.

[9] B. Pholjaroen, N. Li, J. Yang, G. Li, W. Wang, A. Wang, Y. Cong, X. Wang, T. Zhang, Production of renewable jet fuel range branched alkanes with xylose and methyl isobutyl ketone, Industrial and Engineering Chemistry Research. 53 (2014) 13618–13625. https://doi.org/10.1021/ie5016365.

[10] J.D. Lewis, S. Van De Vyver, Y. Román-Leshkov, Acid-Base Pairs in Lewis Acidic Zeolites Promote Direct Aldol Reactions by Soft Enolization, Angewandte Chemie - International Edition. 54 (2015) 9835–9838. https://doi.org/10.1002/anie.201502939.

[11] M. Su, W. Li, T. Zhang, H.S. Xin, S. Li, W. Fan, L. Ma, Production of liquid fuel intermediates from furfural via aldol condensation over Lewis acid zeolite catalysts, Catalysis Science and Technology. 7 (2017) 3555–3561. https://doi.org/10.1039/c7cy01028a.

[12] R.M. West, Z.Y. Liu, M. Peter, J.A. Dumesic, Liquid alkanes with targeted molecular weights from biomass-derived carbohydrates., ChemSusChem. 1 (2008) 417–424. https://doi.org/10.1002/cssc.200800001.

[13] W. Shen, G.A. Tompsett, K.D. Hammond, R. Xing, F. Dogan, C.P. Grey, W.C. Conner, S.M. Auerbach, G.W. Huber, Liquid phase aldol condensation reactions with MgO-ZrO2 and shape-selective nitrogen-

substituted NaY, Applied Catalysis A: General. 392 (2011) 57–68. https://doi.org/10.1016/j.apcata.2010.10.023.

[14] H. Olcay, A. V. Subrahmanyam, R. Xing, J. Lajoie, J.A. Dumesic, G.W. Huber, Production of renewable petroleum refinery diesel and jet fuel feedstocks from hemicellulose sugar streams, Energy and Environmental Science. 6 (2013) 205–216. https://doi.org/10.1039/c2ee23316a.

[15] Q. Liu, X. Zhang, Q. Zhang, Q. Liu, C. Wang, L. Ma, Synthesis of Jet Fuel Range Cycloalkanes with Cyclopentanone and Furfural, Energy and Fuels. 34 (2020) 7149–7159. https://doi.org/10.1021/acs.energyfuels.0c00919.

[16] M. Hronec, K. Fulajtárova, T. Liptaj, M. Štolcová, N. Prónayová, T. Soták, Cyclopentanone: A raw material for production of C15 and C17 fuel precursors, Biomass and Bioenergy. 63 (2014) 291–299. https://doi.org/10.1016/j.biombioe.2014.02.025.

[17] Q. Liu, C. Zhang, N. Shi, X. Zhang, C. Wang, L. Ma, Production of renewable long-chained cycloalkanes from biomass-derived furfurals and cyclic ketones, RSC Advances. 8 (2018) 13686–13696. https://doi.org/10.1039/c8ra01723a.

[18] W. Wang, X. Ji, H. Ge, Z. Li, G. Tian, X. Shao, Q. Zhang, Synthesis of C15 and C10 fuel precursors with cyclopentanone and furfural derived from hemicellulose, RSC Advances. 7 (2017) 16901–16907. https://doi.org/10.1039/c7ra02396k.

[19] J. Yang, N. Li, G. Li, W. Wang, A. Wang, X. Wang, Y. Cong, T. Zhang, Solvent-free synthesis of C10 and C11 branched alkanes from furfural and methyl isobutyl ketone, ChemSusChem. 6 (2013) 1149–1152. https://doi.org/10.1002/cssc.201300318.

[20] X. Kong, X. jie Wei, L. ping Li, Z. Fang, H. Lei, Production of liquid fuel intermediates from furfural via aldol condensation over La2O2CO3-ZnO-Al2O3 catalyst, Catalysis Communications. 149 (2021) 106207. https://doi.org/10.1016/j.catcom.2020.106207.

[21] Y. Zhao, M. Fan, P. Wang, C. Li, L. Wang, L. Wang, Hydrophobic strong solid base derived from graphene oxide hybrid zirconium MOFs and its enhanced stability on furfural-MIBK aldol condensation to synthesize branched biofuel precursors, Fuel Processing Technology. 198 (2020) 106250. https://doi.org/10.1016/j.fuproc.2019.106250.

[22] H.C. Zhou, J.R. Long, O.M. Yaghi, Introduction to metal-organic frameworks, Chemical Reviews. 112 (2012) 673–674. https://doi.org/10.1021/cr300014x.

[23] N. Stock, S. Biswas, Synthesis of metal-organic frameworks (MOFs): Routes to various MOF topologies, morphologies, and composites, Chemical Reviews. 112 (2012) 933–969. https://doi.org/10.1021/cr200304e.

[24] A. Bavykina, N. Kolobov, I.S. Khan, J.A. Bau, A. Ramirez, J. Gascon, Metal-Organic Frameworks in Heterogeneous Catalysis: Recent Progress, New Trends, and Future Perspectives, Chemical Reviews. 120 (2020) 8468–8535. https://doi.org/10.1021/acs.chemrev.9b00685.

[25] L. Zhu, X.Q. Liu, H.L. Jiang, L.B. Sun, Metal-Organic Frameworks for Heterogeneous Basic Catalysis, Chemical Reviews. 117 (2017) 8129–8176. https://doi.org/10.1021/acs.chemrev.7b00091.

[26] A. Herbst, C. Janiak, MOF catalysts in biomass upgrading towards value-added fine chemicals, CrystEngComm. 19 (2017) 4092–4117. https://doi.org/10.1039/c6ce01782g.

[27] R. Fang, A. Dhakshinamoorthy, Y. Li, H. Garcia, Metal organic frameworks for biomass conversion, Chemical Society Reviews. 49 (2020) 3638–3687. https://doi.org/10.1039/d0cs00070a.

[28] J.H. Cavka, S. Jakobsen, U. Olsbye, N. Guillou, C. Lamberti, S. Bordiga, K.P. Lillerud, A new zirconium inorganic building brick forming metal organic frameworks with exceptional stability, Journal of the American Chemical Society. 130 (2008) 13850–13851. https://doi.org/10.1021/ja8057953.

[29] H. Wu, T. Yildirim, W. Zhou, Exceptional mechanical stability of highly porous zirconium metal-organic framework UiO-66 and its important implications, Journal of Physical Chemistry Letters. 4 (2013) 925–930. https://doi.org/10.1021/jz4002345.

[30] J. Winarta, B. Shan, S.M. McIntyre, L. Ye, C. Wang, J. Liu, B. Mu, A Decade of UiO-66 Research: A Historic Review of Dynamic Structure, Synthesis Mechanisms, and Characterization Techniques of an Archetypal Metal-Organic Framework, Crystal Growth and Design. 20 (2020) 1347–1362. https://doi.org/10.1021/acs.cgd.9b00955.

[31] Y. Feng, Q. Chen, M. Jiang, J. Yao, Tailoring the Properties of UiO-66 through Defect Engineering: A Review, Industrial and Engineering Chemistry Research. 58 (2019) 17646–17659. https://doi.org/10.1021/acs.iecr.9b03188.

[32] S. Yuan, J.S. Qin, C.T. Lollar, H.C. Zhou, Stable Metal-Organic Frameworks with Group 4 Metals: Current Status and Trends, ACS Central Science. 4 (2018) 440–450. https://doi.org/10.1021/acscentsci.8b00073.

[33] M.J. Cliffe, W. Wan, X. Zou, P.A. Chater, A.K. Kleppe, M.G. Tucker, H. Wilhelm, N.P. Funnell, F.X. Coudert, A.L. Goodwin, Correlated defect nanoregions in a metal-organic framework, Nature Communications. 5 (2014) 1–8. https://doi.org/10.1038/ncomms5176.

[34] A. Osatiashtiani, A.F. Lee, M. Granollers, D.R. Brown, L. Olivi, G. Morales, J.A. Melero, K. Wilson, Hydrothermally Stable, Conformal, Sulfated Zirconia Monolayer Catalysts for Glucose Conversion to 5-HMF, ACS Catalysis. 5 (2015) 4345–4352. https://doi.org/10.1021/acscatal.5b00965.

[35] D. Zhao, J. Feng, Q. Huo, N. Melosh, G.H. Fredrickson, B.F. Chmelka, G.D. Stucky, Triblock copolymer syntheses of mesoporous silica with periodic 50 to 300 angstrom pores, Science. 279 (1998) 548–552. https://doi.org/10.1126/science.279.5350.548.

[36] J.A. Melero, L.F. Bautista, J. Iglesias, G. Morales, R. Sánchez-Vázquez, Zr-SBA-15 acid catalyst: Optimization of the synthesis and reaction conditions for biodiesel production from low-grade oils and fats, Catalysis Today. 195 (2012) 44–53. https://doi.org/10.1016/j.cattod.2012.04.025.

[37] M. Paniagua, G. Morales, J.A. Melero, J. Iglesias, C. López-Aguado, N. Vidal, R. Mariscal, M. López-Granados, I. Martínez-Salazar, Understanding the role of Al/Zr ratio in Zr-Al-Beta zeolite: towards the one-pot production of GVL from glucose, Catalysis Today. (2020). https://doi.org/10.1016/j.cattod.2020.04.025.

[38] J.A. Melero, G. Morales, J. Iglesias, M. Paniagua, C. López-Aguado, Rational Optimization of Reaction Conditions for the One-Pot Transformation of Furfural to γ-Valerolactone over Zr–Al-Beta Zeolite: Toward the Efficient Utilization of Biomass, Industrial & Engineering Chemistry Research. (2018) acs.iecr.8b02475. https://doi.org/10.1021/acs.iecr.8b02475.

[39] H. Hattori, Heterogeneous Basic Catalysis, Chemical Reviews. 95 (1995) 537–558. https://doi.org/10.1021/cr00035a005.

[40] Y. Tang, J. Xu, X. Gu, Modified calcium oxide as stable solid base catalyst for Aldol condensation reaction, Journal of Chemical Sciences. 125 (2013) 313–320. https://doi.org/10.1007/s12039-013-0362-5.

[41] T. Viinikainen, H. Rönkkönen, H. Bradshaw, H. Stephenson, S. Airaksinen, M. Reinikainen, P. Simell, O. Krause, Acidic and basic surface sites of zirconia-based biomass gasification gas clean-up catalysts, Applied Catalysis A: General. 362 (2009) 169–177. https://doi.org/10.1016/j.apcata.2009.04.037.

[42] J. Iglesias, J.A. Melero, G. Morales, M. Paniagua, B. Hernández, A. Osatiashtiani, A.F. Lee, K. Wilson, ZrO2-SBA-15 catalysts for the one-pot cascade synthesis of GVL from furfural, Catalysis Science and Technology. 8 (2018) 4485–4493. https://doi.org/10.1039/c8cy01121d.

[43] R. Wei, C.A. Gaggioli, G. Li, T. Islamoglu, Z. Zhang, P. Yu, O.K. Farha, C.J. Cramer, L. Gagliardi, D. Yang, B.C. Gates, Tuning the Properties of Zr 6 O 8 Nodes in the Metal Organic Framework UiO-66 by Selection of Node-Bound Ligands and Linkers, Chemistry of Materials. 31 (2019) 1655–1663. https://doi.org/10.1021/acs.chemmater.8b05037.

[44] J. Jae, G.A. Tompsett, A.J. Foster, K.D. Hammond, S.M. Auerbach, R.F. Lobo, G.W. Huber, Investigation into the shape selectivity of zeolite catalysts for biomass conversion, Journal of Catalysis. 279 (2011) 257–268. https://doi.org/10.1016/j.jcat.2011.01.019.

[45] K.G. Joback, R.C. Reid, Estimation of Pure-Component Properties from Group-Contributions, Chemical Engineering Communications. 57 (1987) 233–243. https://doi.org/10.1080/00986448708960487.

[46] C. López-Aguado, M. Paniagua, J. Iglesias, G. Morales, J.L. García-Fierro, J.A. Melero, Zr-USY zeolite: Efficient catalyst for the transformation of xylose into bio-products, Catalysis Today. 304 (2018) 80–88. https://doi.org/10.1016/j.cattod.2017.08.031.

[47] Y. Wang, L. Li, P. Dai, L. Yan, L. Cao, X. Gu, X. Zhao, Missing-node directed synthesis of hierarchical pores on a zirconium metal-organic framework with tunable porosity and enhanced surface acidity: Via a microdroplet flow reaction, Journal of Materials Chemistry A. 5 (2017) 22372–22379. https://doi.org/10.1039/c7ta06060b.

[48] V.R. Bakuru, S.R. Churipard, S.P. Maradur, S.B. Kalidindi, Exploring the Brønsted acidity of UiO-66 (Zr, Ce, Hf) metal-organic frameworks for efficient solketal synthesis from glycerol acetalization, Dalton Transactions. 48 (2019) 843–847. https://doi.org/10.1039/c8dt03512a.

[49] M. Muñoz-Olasagasti, A. Sañudo-Mena, J.A. Cecilia, M.L. Granados, P. Maireles-Torres, R. Mariscal, Direct Conversion of Levulinic Acid into Valeric Biofuels Using Pd Supported Over Zeolites as Catalysts, Topics in Catalysis. 62 (2019) 579–588. https://doi.org/10.1007/s11244-019-01147-4.

[50] K. Chakarova, I. Strauss, M. Mihaylov, N. Drenchev, K. Hadjiivanov, Evolution of acid and basic sites in UiO-66 and UiO-66-NH2 metal-organic frameworks: FTIR study by probe molecules, Microporous and Mesoporous Materials. 281 (2019) 110–122. https://doi.org/10.1016/j.micromeso.2019.03.006.

[51] R.C. Klet, Y. Liu, T.C. Wang, J.T. Hupp, O.K. Farha, Evaluation of Brønsted acidity and proton topology in Zr- and Hf-based metal-organic frameworks using potentiometric acid-base titration, Journal of Materials Chemistry A. 4 (2016) 1479–1485. https://doi.org/10.1039/c5ta07687k.

[52] O. Kikhtyanin, D. Kubička, J. Čejka, Toward understanding of the role of Lewis acidity in aldol condensation of acetone and furfural using MOF and zeolite catalysts, Catalysis Today. 243 (2015) 158–162. https://doi.org/10.1016/j.cattod.2014.08.016.

[53] G.E.P. Box, J.S. Hunter, W.G. Hunter, Statistics for Experimenters: Design, Innovation, and Discovery, 2nd Edition, Wiley, 2005. https://www.wiley.com/en-us/9780471718130 (accessed March 20, 2021).